

Molecular Simulation of Liquids and Gels

Alex Malins

Bristol Centre for Complexity Sciences, University of Bristol, Bristol, BS8 1TS, UK

Supervision by Dr. C. Patrick Royall, Department of Chemistry, University of Bristol, and Prof Jens Eggers, School of Mathematics, University of Bristol.

Abstract

The combination of long range structural disorder and strong interactions means the liquid phase is not as well understood as the other principle states of matter. The development of liquid state theory has been slow as a consequence [1]. The internal structure of a liquid is random when viewed on a large scale, but also displays ordering on a local scale. In particular the importance of energetically favourable clusters of particles called locally favoured structures (LFS) to local ordering was discussed by Sir Charles Frank in 1952 [2]. I simulate a fluid of Lennard-Jones particles [3] to examine the internal structure near the phase boundary using molecular dynamics [4] A novel method called topological cluster classification [5] is used to identify LFS in the bulk. I disprove a 1952 conjecture by Frank regarding the populations of icosahedral LFS in liquids, but find encouraging signals coupling LFS to the process of crystallization and dynamical arrest.

Colloidal dispersions are ensembles of microscopic particles suspended in a solvent which display dynamics with similar phase behaviour to simple atomic and molecular systems. Under certain conditions they form metastable solids such as glasses, gels and crystals. I simulate the formation of colloidal gels in experimental dispersions [6] using a basic model for inter-colloidal interactions [7, 8] and Brownian dynamics [9]. I find the simulation results do not match the gelation witnessed in the experiments and discuss why this discrepancy arises.

Contents

1	Introduction	3
1.1	The Liquid State	3
1.2	Lennard-Jones Clusters	3
1.3	Colloids and Gelation	5
2	Methods	7
2.1	Molecular Dynamics Simulation of Canonical Lennard Jones Fluids	7
2.2	Topological Cluster Classification (TCC)	9
2.3	Simulations of the Experimental Dispersions	10
2.4	Brownian Dynamics Simulation of Gel Percolation	11
2.5	Classification of State Points as Gels, Fluids and Cluster Fluids	12
3	Results	14
3.1	Lennard-Jones Fluid Cluster Analysis	14
3.2	Brownian Dynamics Simulation of Gels	18
4	Conclusions and Future Research Directions	20
5	Acknowledgments	22

1 Introduction

1.1 The Liquid State

The study of the liquid state has a long and rich history as scientists have sought to understand the structural nature of this phase. Intuitively liquids are perceived as being an intermediate state between gases and solids. They flow like gases and the constituents interact strongly like solids, yet the structure does not display long-range order like a crystal. These factors have acted to slow the development of liquid state theories [1].

Materials science is a discipline which studies systems at the atomic or molecular scale and relates the microscopic structure and dynamics to observable macroscopic properties. This report limits its scope to classical systems, which includes ensembles of all but the lightest of atoms or molecules (He, H₂, D₂, etc) and systems where vibrational motion is such that $h\nu \ll k_B T$ [4].

Simple liquids are often well described by a single inter-particle interaction potential. The total force on a particle is derived from the system Hamiltonian and application of Newton's Second Law yields the ordinary differential equations (ODEs) governing the motion of the constituents. The sheer number of particles in systems considered by material scientists means there is usually no analytical solution the ODEs.

Theories have been developed to describe the equilibrium properties of fluids in macroscopic terms, where constituent particles are treated statistically. Approximations are requisite for all but the simplest systems such as the ideal gas, the harmonic crystal and the two-dimensional Ising model for ferromagnets [4]. It is now possible to compute a numerical solution of the ODEs to any desired accuracy. The technique to do this is known as molecular dynamics and its only limitation is the speed at which the computing resource is able to crunch the numbers [9].

1.2 Lennard-Jones Clusters

A model proposed by Sir John Lennard-Jones in the 1920s to simulate simple atomic liquids employs a Lennard-Jones interaction between atoms [3]. The interaction is an approximation to the theoretical interatomic potential for an Argon fluid, where atoms attract at long ranges and strongly repel for separations shorter than one atomic diameter. An extensive computational study of the phases of the Lennard-Jones system was conducted by Hansen and Verlet in 1969 [10]. Molecular dynamics yields the trajectories of all particles in a fluid ensemble which can be used for structural analysis of non-ergodic phases and to develop theory for non-equilibrium dynamics.

In 1952 Sir Charles Frank proposed the idea that local groupings, or clusters, of particles may be influential during dynamical arrest of a liquid [2]. He proposed a thought experiment on the arrangements of twelve billiard balls arranged in contact with a single central billiard. An arrangement is considered distinct if it cannot be transformed into another without an outer billiard breaking contact with the central one. Three distinct arrangements exist. Two are fragments of a bulk crystal with either face-centred cubic (FCC) or hexagonal close-packed (HCP) structure. A third arrangement is constructed if each of the outer billiards is placed at the vertices of a regular icosahedron.

If the billiards are deformable like atoms, the outer billiards of the icosahedron would lie fractionally closer to the centre than in the crystal formations. To quantify this difference, thirteen Lennard-Jones particles arranged as an icosahedron would have an 8.4% higher binding energy than either of the crystal fragments. He states that the icosahedral grouping should manifest in clusters of particles in Lennard-Jones liquids:

I infer that this (icosahedral arrangement) will be a very common grouping in liquids, that most of the groups of twelve atoms around one in this form.

This conjecture is tested directly in this report.

Frank goes on to discuss the consequences of icosahedral ordering when a liquid is cooled below the freezing line. If one attempts to construct a three-dimensional solid from building blocks of icosahedra the resulting bulk would contain voids as the icosahedra do not tessellate. Consequently crystals have a higher binding energy per particle when averaged over the whole solid. In order for a supercooled liquid to crystallize, substantial rearrangement of particles at a local level must occur and this is costly in terms of energy. The system may undergo dynamical arrest, or vitrification, in preference to crystallization. This is when liquid

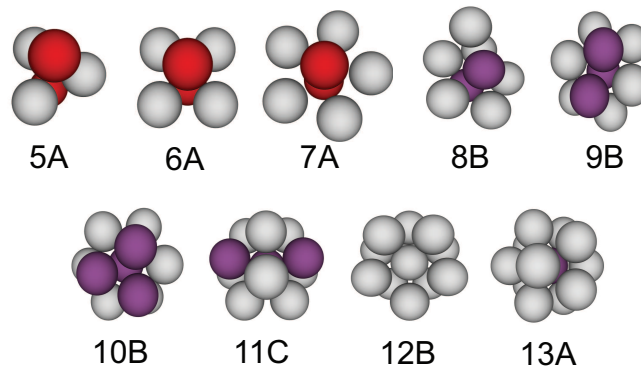


Fig. 1: **The nine Lennard-Jones $m = 5$ to $m = 13$ locally favoured structures (LFS).** Structure 13A is identical to the icosahedral arrangement of thirteen billiards Frank discusses. Its five-fold symmetry means there is an energy penalty for incorporation into a crystal bulk. Other structures with geometries energetically unfavourable for crystal growth include the pentagonal-bipyramids 7A, 8B, 9B and 10B [18]. Structure 6A is a fragment of a crystal.

flow halts and the system jams a non-ergodic phase, such as a glass or a gel, with no long-range structural order.

Research has been conducted to detect the presence of icosahedral groupings in both simulated and experimental fluids. Icosahedra possess a five-fold symmetry unlike crystal structures. Steinhardt, Nelson and Ronchetti used bond-orientational order parameters to detect five-fold symmetry in clusters of particles in Lennard-Jones liquids and glasses [11]. They note an increase in five-fold symmetry in supercooled liquids 10% below the freezing line. Extensions to this research have associated five-fold symmetry with dynamical arrest [12, 13, 14], while experiments have identified five-fold symmetry at interfaces [15], and in the bulk [16].

There is a natural extension of Frank's analysis to include clusters formed of any number of particles. The structural arrangement of n isolated particles with greatest binding energy is termed a locally favoured structure (LFS). For a given potential this may be a crystal fragment, or be a structure with a large energy barrier to reordering as a crystal fragment. If the latter is the case an energy landscape interpretation of system phase indicates this will have an effect on crystallization [17]. If a liquid on the freezing line contains a sizable proportion of clusters with a high energy barrier for conversion to crystal fragments they may act to impede crystallization and promote vitrification.

In this paper I consider LFS of $m = 5$ to $m = 13$ units in size. There are 22 LFS of these for the variable range Morse interaction and the structures are given in [18]. The nine $m = 5$ to $m = 13$ LFS associated with the Lennard Jones potential are a subset of the 22 Morse LFS, and correspond to the LFS of the Morse interaction with range parameter $\rho_0 = 6$ (see eq 10) [18]. The structures of the Lennard-Jones LFS are depicted in figure 1.

The Lennard-Jones global minimum for seven atoms is the 7A structure, where particles are arranged at the vertices of a pentagonal-bipyramid. 8B is a 7A pentagonal-bipyramid with an additional atom attached, whilst 9B and 10B are composed respectively of an overlapping pair or triplet of 7A pentagonal-bipyramids. These four structures are known to be topologically dissimilar to crystal packings and are thought to impede crystallization of bulk fluids [17]. The six particle 6A structure is topologically similar to crystal fragments of the same size and so permits crystallization.

I simulate Lennard-Jones fluids using molecular dynamics. I then utilize a new algorithm called topological cluster classification (TCC) to identify local structure present in coordinate snapshots of the ensemble [5]. It detects the particles that are members of the 22 Morse LFS, and the two $m = 13$ particle crystal clusters. From hereon I call these 24 structures the *Morse clusters*. The nine global minima Lennard-Jones LFS and the two $m = 13$ crystal clusters are collectively known as the *Lennard-Jones clusters*. I examine the populations of all these clusters in the simulation liquids. More details on the TCC algorithm can be found in section 2.2 or [5].

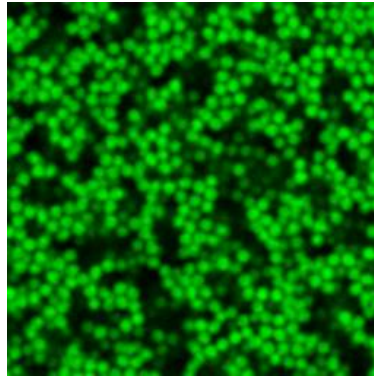


Fig. 2: An image of colloidal gel from [6]. Generated with a confocal microscope.

From the simulations I note that the proportion of particles identified in clusters increases and that cluster life-time grows as the liquid is cooled towards the freezing line. In other words fluids order locally upon cooling and the structures formed stabilize. I find Frank incorrect with his assertion that the most common groupings of twelve particles around one would be icosahedral; it is in fact the FCC crystal cluster. However in themselves thirteen particle clusters are found to be relatively rare. Most particles are detected as members of smaller clusters.

The two most common structures found on the freezing line are $8B$ and $9B$ pentagonal-bipyramids, whose particles account for almost 40% of all the particles detected in the Lennard-Jones clusters. It is plausible that due to sheer population size, the pentagonal-bipyramid based LFS are more important to the process of vitrification than icosahedra.

1.3 Colloids and Gelation

Colloidal dispersions are a suspension of micron scale particles, or colloids, suspended in a fluid solvent. They are prevalent in many consumer products, for example in foodstuffs such as mayonnaise and yoghurts [19], and in inks and paints [20]. Also known as colloidal suspensions, they display dynamics similar to many atomic systems due to the Brownian motion of the colloids. They are attractive systems to employ in experimental studies due to numerous practical advantages over working with atomic systems. Characteristic length and timescales of colloidal systems are much larger, meaning individual particles can be observed directly by confocal microscope [21]. The dynamics occur on amenable (laboratory) time scales and colloids are small enough that thermal energy $k_B T$ drives dynamics. The interactions between colloids can be engineered to almost arbitrary degree, whereas atomic interactions are dictated by elementary chemistry.

Colloidal suspensions consisting of a great number of components and with complex non-equilibrium behaviour can often be well described by a single effective potential between particles. This is because the additional degrees of freedom introduced by the solvent generally evolve much faster than the colloids and can often be “integrated out” [22]. The fundamental simplicity of some of the interactions perhaps belies interesting ergodic and non-ergodic states displayed by large ensembles of colloids in a dispersion.

Recently attention has been paid to understanding the process in which colloidal suspensions undergo gelation [23]. Gels are a metastable state created when low density dispersions are cooled below the freezing temperature and undergo dynamical arrest. During the arrest particles flocculate to form a three-dimensional semi-rigid network. Gels are in essence similar to glasses; they are a non-ergodic solid above an underlying thermodynamic ground state of crystal-gas coexistence. However the structure of a gel means it has a much lower yield stress than either a glass or a crystal.

The sheer number of solvent particles for every colloid makes simulation of dispersions with molecular dynamics very expensive. Small time-steps are required to capture the relatively fast dynamics of the solvent and long runs needed to allow evolution of the slow colloids. The Brownian dynamics simulation was developed as a solution to problems of this type [24], where solvent particles are omitted from direct simulation and

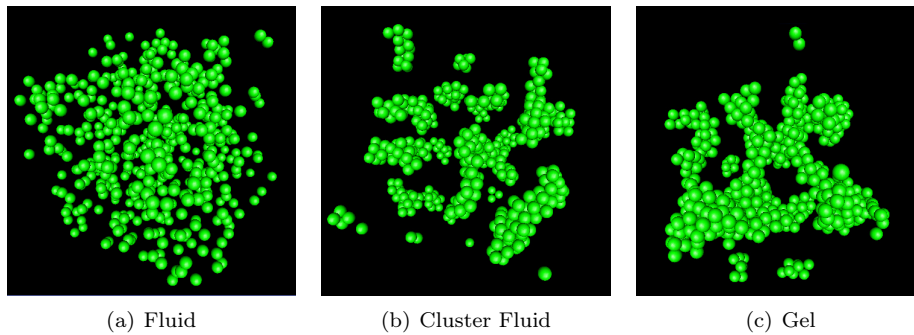


Fig. 3: **Simulation images of colloidal dispersions in a) fluid, b) cluster fluid and c) gel phases.** Generated with parameters a) ($\phi_c = 0.05, \epsilon = 2$), b) ($\phi_c = 0.05, \epsilon = 10$) and c) ($\phi_c = 0.10, \epsilon = 10$).

their effect on the colloids is reduced to a set of random forces.

The simulations I present are parametrized to model experimental observations of gelation in Royall et al. [6]. I sample state points from the phase space of a model for the experimental dispersion. The two degrees of freedom defining the phase space are analogous to density and temperature for the Lennard-Jones system¹. Volume fraction $\phi_c = \frac{V_c}{V}$ is the proportion of the total simulation volume occupied by colloids and is analogous to number density $\rho = \frac{N}{V}$ of a Lennard-Jones ensemble. The strength of the interaction potential between colloids, ϵ , alters the dynamics of the colloidal system akin to a temperature change in a Lennard-Jones system. A strong interaction dominates the Brownian motion of the colloids similar to how thermal energy $k_B T$ decreases in importance as particles form stable bonds at low temperatures in Lennard-Jones systems.

Depending on the observed dynamics, the experimental and simulation state points are categorized in three ways. In fluids the thermal energy $k_B T$ of the particles dominates interaction strength and little structural ordering arises. Any structure witnessed is generally only local and short lived so a random ensemble is observed, figure 3a. The second category is for cluster fluids which are composed of rigid clumps of particles with glassy structure akin to glasses which flow freely within the solvent, figure 3b. Thirdly I consider gels which are a percolated network of clumps of a cluster fluid forming a low-density solid seen in figure 3c.

Cluster fluids and gels are observed in the fluid-crystal coexistence region of the dispersion phase diagram. The region is bounded by the phase separation line which can be calculated by free-volume theory [25]. It is noted that gels generally form at higher volume fractions ϕ_c than cluster fluids and this defines a percolation line for gelation through the coexistence region. I sample simulation state points to map the position of this in phase space. I find that the location of the simulation percolation line lies at a higher volume fraction ϕ_c than in the experiments. This indicates an inaccuracy in the model for the dispersion which is discussed in the conclusion.

¹ A density-temperature phase diagram for the Lennard Jones system was calculated by Hansen [10].

2 Methods

2.1 Molecular Dynamics Simulation of Canonical Lennard Jones Fluids

I simulate an ensemble of N particles interacting via the pairwise 12-6 Lennard-Jones potential [3]. For two particles, each of mass m and separated by a Euclidean distance r , this is given by

$$V_{LJ}(r) = 4\epsilon \left[\left(\frac{\sigma}{r} \right)^{12} - \left(\frac{\sigma}{r} \right)^6 \right]. \quad (1)$$

In isolation the two particles would be at equilibrium when separated by distance $r = 2^{\frac{1}{6}}\sigma$, with ϵ being the bond energy for this separation. It has been shown that the equilibrium properties of an ensemble of Lennard-Jones particles is very similar to those of argon with parameters $\sigma = 3.405$, $\frac{\epsilon}{k_B} = 119.8K$ [10].

It is more convenient to work with dimensionless quantities when one is interested in the qualitative behaviour of the Lennard-Jones system. My simulations calculate on reduced units where the constants m , ϵ , σ , and k_B are set to unity and any other quantities are measured as multiples of these.

$$m = \epsilon = \sigma = k_b = 1. \quad (2)$$

For reasons of computational efficiency, the potential is truncated for separations greater than $r_c = 2.5$. I shift the potential such that no discontinuity occurs.

$$V_{comp}(r) = \begin{cases} 4 \left(\frac{1}{r^{12}} - \frac{1}{r^6} \right) - 4 \left(\frac{1}{r_c^{12}} - \frac{1}{r_c^6} \right) & r < r_c \\ 0 & r \geq r_c \end{cases}. \quad (3)$$

The force acting on particle i due to a particle j at a distance r_{ij} is given by eq 4, where $\hat{\mathbf{r}}_{ij}$ is the unit vector oriented from particle i to j .

$$\mathbf{F}_{ij}(\mathbf{r}_{ij}) = \begin{cases} 24 \left(\frac{2}{r_{ij}^{13}} - \frac{1}{r_{ij}^7} \right) \hat{\mathbf{r}}_{ij} & r_{ij} < r_c \\ 0 & r_{ij} \geq r_c \end{cases}. \quad (4)$$

A Nosé-Hoover Thermostat is employed to constrain the thermodynamic temperature of the ensemble [26]. The derivation of the thermostat introduces an additional degree of freedom ξ to the system. This evolves subject to an ODE which couples to the equations of motion of the particles (equation 7). This is analogous to the incorporation of a heat reservoir in physical experiments. When the instantaneous simulation temperature strays from a desired temperature T_D , which is incorporated as a parameter into the thermostat, the particles exchange kinetic energy with the reservoir. The magnitude of the exchange is a dependent on parameter Q called the reservoir coupling constant. Intuitively $\frac{1}{Q}$ is the size of the heat bath - a small value of Q leads to large heat exchange of heat between the ensemble and the reservoir given a temperature difference. In my simulations $Q = 1$.

$$\dot{\mathbf{r}}_i = \mathbf{p}_i, \quad (5)$$

$$\dot{\mathbf{p}}_i = \sum_{j=1, j \neq i}^N \mathbf{F}_{ij}(\mathbf{r}_{ij}) - \xi \mathbf{p}_i, \quad (6)$$

$$\dot{\xi} = \frac{1}{Q} \left(\sum_{j=1}^N \mathbf{p}_j^2 - \frac{3N}{T_D} \right). \quad (7)$$

A molecular dynamics simulation involves integrating ordinary differential equations 5, 6 and 7 to give numerical trajectories $\{\mathbf{r}_i, \mathbf{p}_j\}$ for the particles. Time is discretized into steps of length δt , called time-steps. The positions and momenta of all the particles and ξ , are updated simultaneously between time-steps using an integrator. The instantaneous simulation temperature T is defined as

$$T = \frac{1}{3N} \sum_{j=1}^N \mathbf{p}_j^2, \quad (8)$$

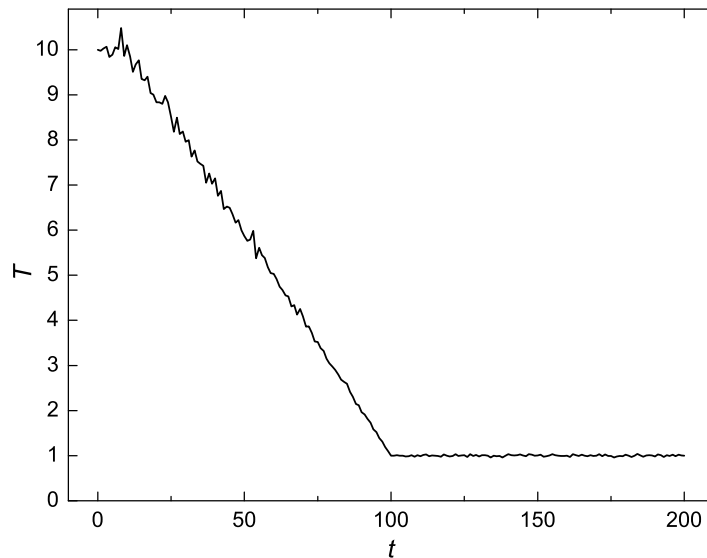


Fig. 4: **Graph of simulation temperature for the equilibration phase of a simulation. Step 1**, random initialization of ensemble at $\rho = 0.85$ and $T = 10.00$. **Step 2**, high temperature equilibration for first $10t$ of simulation. **Step 3**, linear cooling of ensemble with thermostat to final temperature $T \simeq T_F$, where $T_F = 1$ in figure shown. **Step 4**, a further $100t$ of equilibration before examination of the liquid structure begins.

where particle velocities $\mathbf{p}_j = \mathbf{p}_j(t)$.

The dependence of a particle's acceleration on the velocities of all particles (equation 6 reads $\dot{\mathbf{p}}_i = \mathbf{g}(\mathbf{r}_j, \mathbf{p}_j, \xi)$) prohibits the use of symplectic Verlet-based integrators traditionally employed in molecular dynamics. These were preferred as the total energy of the system was bounded during the simulation [9], however this requirement is unnecessary for canonical NVT simulations as the simulation temperature T is constrained by the thermostat. The 4th-order Runge-Kutta numerical integration scheme is employed instead, equation 9. For initial value problems of the form $\dot{\mathbf{x}}_i(t) = \mathbf{g}(\mathbf{x}_j(t), \mathbf{y}_j(t), z(t))$, like equations 5, 6 and 7, $\mathbf{x}_i(t + \delta t)$ is given by

$$\mathbf{x}_i(t + \delta t) = \mathbf{x}_i(t) + \frac{\delta t}{6}(k_1 + 2k_2 + 2k_3 + k_4), \quad (9)$$

where j denotes all particles and

$$\begin{aligned} k_1 &= \mathbf{g}(\mathbf{x}_j(t), \mathbf{y}_j(t), z(t)), \\ k_2 &= \mathbf{g}(\mathbf{x}_j(t + \frac{\delta t}{2}k_1), \mathbf{y}_j(t + \frac{\delta t}{2}k_1), z(t + \frac{\delta t}{2}k_1)), \\ k_3 &= \mathbf{g}(\mathbf{x}_j(t + \frac{\delta t}{2}k_2), \mathbf{y}_j(t + \frac{\delta t}{2}k_2), z(t + \frac{\delta t}{2}k_2)), \\ k_4 &= \mathbf{g}(\mathbf{x}_j(t + \delta tk_3), \mathbf{y}_j(t + \delta tk_3), z(t + \delta tk_3)). \end{aligned}$$

The fluids are simulated in a cube of side $\sqrt[3]{V}$, where the volume V is chosen such that the number density $\rho = \frac{N}{V}$ is fixed. To eliminate any surface effects periodic boundary conditions are implemented: the simulation box is replicated throughout space forming an infinite lattice and whenever a particle leaves through any face of the box, a periodic image of the particle enters through the opposing face. This conserves the position of the centre of mass of the system.

Computer simulations have shown that the triple point of a Lennard Jones fluid is at $T_\tau = 0.68 \pm 0.02$, $\rho_\tau = 0.85 \pm 0.01$ [10]. Particles are randomly inserted into a box of density $\rho = 0.573$. The box is then crushed to a density $\rho = 0.85$ whilst ensuring no two particles encroach by a distance less than 1. All simulations are executed at constant density ($\rho = 0.85$) above the triple points. This allows me to examine the slowest

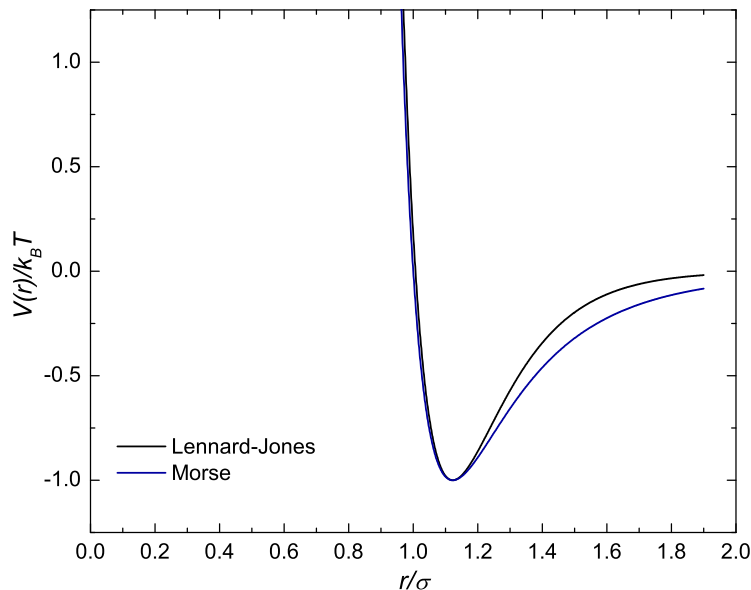


Fig. 5: **Comparison of the Lennard-Jones and Morse interactions.** The Morse potential is plotted with range parameter $\rho_0 = 6$ and mean bond separation $r_e = 2^{\frac{1}{6}}\sigma$. Lennard-Jones takes $\epsilon = k_B T$. Both interactions are qualitatively similar, and have topologically identical global minimum clusters of $m = 5$ to $m = 13$ particles in size.

permitted dynamics for an equilibrium Lennard-Jones liquid. The velocities are initialized randomly, subject to the constraint that the initial temperature of the ensemble is $T = 10.00$.

I simulate 2048 particle Lennard-Jones fluids. Let simulation time be denoted t . The simulations begin with an equilibration process. Firstly the system is homogenized as a high temperature fluid, $T_{hot} = 10.00$, for 10^4 time-steps where the kinetic energy of the particles dominates the pairwise interactions. The dynamics here are diffusive and any structural ordering originating from the zero-time configuration is almost entirely destroyed. The system is then cooled linearly at a rate of $10^{-4}t^{-1}$ units per time-step to final temperature T_F above the freezing line. This is achieved by adjusting value of T_D in the thermostat. For example in $9 \cdot 10^4$ time-steps the system will have cooled from $T \simeq T_{hot} = 10.00$ to $T \simeq T_F = 1.00$. The system is then equilibrated at the final temperature T_F for a further 10^5 time units to settle any temperature fluctuations before TCC investigations into local structure are conducted. For all simulations a time-step of $10^{-4}t$ is chosen and $2 \cdot 10^7$ steps are integrated. Total simulation time is $2000t$ time units. The equilibration process is depicted in figure 4. For comparison this would equate to a simulation roughly $4 \cdot 10^{-9}s \equiv 4ns$ if modeling liquid Argon.

2.2 Topological Cluster Classification (TCC)

The Morse potential between two like particles at a distance r reads [27]

$$\beta V_M(r) = \epsilon e^{\rho_0(r_e - r)} (e^{\rho_0(r_e - r)} - 2). \quad (10)$$

The parameter ρ_0 determines the range of the interaction, ϵ is the minimum and r_e is the equilibrium bond length. The Morse potential is qualitatively similar to Lennard-Jones (figure 2.2).

The topological cluster classification (TCC) [5] identifies clusters in the bulk phase which are topologically equivalent to the Morse clusters (defined in section 1). The structures of the clusters and their respective binding energies are given in Doye et al [28]. The Lennard Jones LFS are identical to the subset of the Morse clusters, equivalent to the LFS a Morse interaction with range parameter $\rho_0 = 6$. TCC detects all the Morse clusters between sizes $m = 5$ to $m = 13$, including the two 13 particle HCP and FCC crystal fragments.

The methodology of the TCC algorithm is as follows. The first step involves identifying a bond network for the bulk phase using a modified form of Voronoi decomposition [29]. The standard Bernal method detects bonds between adjacent particles regardless of separation. To model finite range interactions Williams [5] introduces a calibration parameter r_k which determines the maximum possible range for a bond. Even though the Lennard-Jones potential is infinite range, the computational potential is truncated so in effect becomes finite range. I set $r_k = 1.8$ for the Lennard-Jones fluids to introduce a notion of strength to a bond. Particles separated by less than $r_k = 1.8$ will have a binding energy at least 10% of the maximum strength bond ϵ for the interaction, whereas particles separated in the range $1.8 < r \leq 2.5$. Two particles separated by less r_k are not automatically identified as bonded however. This is because by nature the Voronoi tessellation is independent of r_k . An explanation of a further perturbation Williams introduces to the Voronoi routine to improve bond detection Williams is found in the original TCC paper [5].

The method moves on to identify the 3, 4 and 5 membered shortest path (SP) rings [30]. These are n membered rings of atoms taken from the bulk of the N particles, where the shortest path through the bulk connecting any pair from a ring utilizes only bonds present in the ring.

The rings are then categorized in three ways:

- those which have one additional particle bonded to all members of the ring,
- those which have two additional particles bonded to all members of the ring,
- those with no such additional particles.

By the construction the bond network means it is impossible to have more than two additional particles bonded to *all* members of the ring. This categorization yields structures which are termed the basic LFS, into which all the $m = 8$ to $m = 13$ Morse global minima LFS and the two 13 particle crystal fragments can be decomposed. A particle is permitted to be a member of more than one basic LFS, i.e. basic LFS may overlap. Examining combinations of the basic LFS enables the TCC algorithm to identify $m = 5$ to $m = 13$ Morse clusters in the bulk. If a particle is found to be part of more than one cluster, it is labeled as attached to the largest of these and associations with smaller clusters are ignored. Again full details on the method can be found in Williams [5].

The detection of individual Morse clusters allows us to directly test Frank's inference that icosahedral 13A clusters will be more common in liquids than thirteen atom FCC and HCP crystal clusters. The TCC algorithm is implemented on the Lennard Jones simulations of section 2.1. On completion of the equilibration phase, TCC is used to detect LFS in 180 subsequent simulation coordinate sets, each separated by $10t$ time units. The $10t$ separation ensures statistical independence of the coordinate samples as, even for the slowest simulation dynamics ($T_F = 0.68$), an average particle will have diffused a distance greater than over the maximum bond length $r_k = 1.8$ (c.f. Fick's law of diffusion in section 2.4).

2.3 Simulations of the Experimental Dispersions

The experiments of Royall et al [6] utilize polymethylmethacrylate colloids in a density matched solvent mixture of cis-decalin and cyclohexyl bromide. The colloids are sterically stabilized and labeled with a fluorescent dye for compatibility with the confocal microscope. The attraction between colloids is created by the depletion effect of a polystyrene polymer added to the solution [22, 31, 8]. Van der Waals interactions are reduced to a fraction of the thermal energy $k_B T$ by matching the refractive index of the colloids and the solvent mixture, and electrostatic interactions are screened by the addition of salt. The colloids have a 4% polydispersity, however this is discounted for the simulations where particles are all of equal diameter.

The experimental dispersion is known to be modeled well by a single pair potential between colloids. This is known as the Asakura-Oosawa (AO) interaction [31]:

$$\beta V_{AO}(r) = \begin{cases} \infty & 0 \leq r < \sigma_c \\ -\eta_p^r \frac{(1+q)^3}{q^3} \left[1 - \frac{3r}{2(1+q)\sigma_c} + \frac{r^3}{2(1+q)^3\sigma_c^3} \right] & \sigma_c \leq r < \sigma_c(1+q) \\ 0 & r \geq \sigma_c(1+q). \end{cases} \quad (11)$$

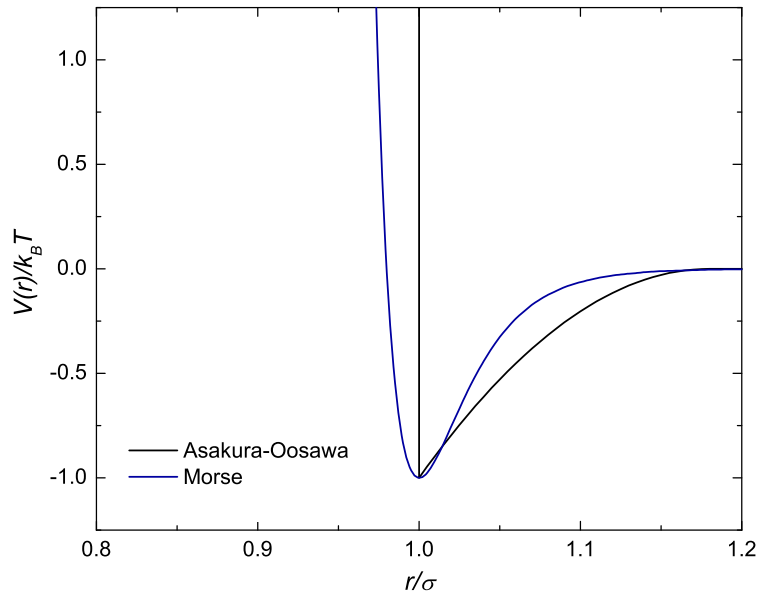


Fig. 6: **Comparison of the theoretical Asakura-Oosawa (AO) potential and Morse interaction.** The latter is implemented in the Brownian dynamics simulations. AO parameters are $\eta_p^r = 35.09$, $q = 0.18$ and Morse are $\rho_0 = 34.38\sigma^{-1}$, $\epsilon = k_B T$, and $r_e = \sigma$. The values $V(r)$ and r quoted in the figure are both reduced by the simulation base units of $k_B T$ and σ respectively.

Constants σ_c and σ_p denote the average diameter of the colloids and the polymer coils respectively. The size ratio $q = \frac{\sigma_p}{\sigma_c}$ sets the range of the interaction. The variable η_p^r is the reservoir packing fraction which determines the depth of the potential and is a linear function of the polymer volume fraction $\phi_p = \frac{V_p}{V}$.

Incorporating the rigid component of the AO interaction ($r < \sigma_c$) into a numerical simulation would require an unphysical correction of coordinates every time particles overlapped. The AO potential is instead approximated by the Morse potential. This is achieved by matching the reduced second virial coefficients of both potentials such that the effective range of the Morse potential is equivalent to the AO range. The procedure to do this is outlined by Noro and Frenkel [32].

The reservoir packing fraction η_p^r fixes the Morse parameters ϵ and ρ_0 . This is undesirable as phase space gains an extra dimension making the task of exploring state points more irksome. I observe that ρ_0 does not vary substantially in the region I wish to sample, so it is fixed as $\rho_0 = 34.38\sigma^{-1}$ for all simulations. This corresponds to an experimental polymer volume fraction $\phi_p = 0.10714$ and $\eta_p^r = 35.09$ (both dimensionless). The simulation phase space is thus reduced to an $\epsilon - \phi_c$ plane. Figure 2.3 shows the mapping of the Morse potential onto the experimental AO potential.

Again it is more convenient to work with reduced units in the Brownian dynamics simulations. All quantities are written in terms of fundamental units σ , $k_B T$ and m . Table 1 converts all the relevant experimental quantities into simulation reduced units.

2.4 Brownian Dynamics Simulation of Gel Percolation

Brownian dynamics is a computer simulation technique used to sample configurations of bi-component systems. It is applicable to systems where one component with fast dynamics interacts with the second in a manner which enables the interactions to be approximated as Brownian noise on the time-scales of the slower mode [9]. This is a natural starting point to describe the effect of a solvent in a colloidal dispersion. The scheme generates a discrete coordinate trajectory \mathbf{r}_i as follows

$$\mathbf{r}_i(t + \delta t) = \mathbf{r}_i(t) + \frac{D}{k_B T} \sum_{j=1, j \neq i}^N \mathbf{F}_{ij}(t) \delta t + \delta \mathbf{r}_i^G. \quad (12)$$

Quantity	Symbol	Experimental SI Value	Simulation Reduced Value
mean colloid diameter	σ	$2.40 \cdot 10^{-6} m$	1
thermal energy (298K)	$k_B T$	$4.11 \cdot 10^{-21} J$	1
mass of colloid	m	$8.66 \cdot 10^{-15} kg$	1
polymer-colloid size ratio	q	0.18	0.18
diffusion constant	D	$7.71 \cdot 10^{-14} m^2 s^{-1}$	$4.66 \cdot 10^{-5} \sigma^{-2} \left(\frac{m\sigma^2}{k_B T} \right)^{0.5}$
time	t	circa 1s	$287.2 \left(\frac{m\sigma^2}{k_B T} \right)^{0.5}$

Tab. 1: **Conversion of physical parameters between SI units and reduced units.** In bold face are the fundamental units in which all other simulation quantities are expressed.

In many ways the methodology of a Brownian dynamics simulation is similar to molecular dynamics. The colloids are allowed to respond to the instantaneous forces present in a given configuration and explore a new configuration δt further in time. Brownian dynamics adds the additional term δr_i^G which models the thermal fluctuations (or Brownian motion) of the colloids arising from the interaction with the solvent. It works by giving each particle a random kick every time-step, where the kick is drawn from a Gaussian distribution with zero mean and variance given by equation 13. The numbers $\delta r_{i\alpha}^G$, the three components of vector δr_i^G , each generated independently.

$$\langle (\delta r_{i\alpha}^G)^2 \rangle = 2D\delta t. \quad (13)$$

The parameter D is the diffusion constant from Fick's second law of diffusion and equation 13 is derived from this.

It is important to understand the implications of the stochastic component of Brownian dynamics. The short term dynamics are unphysical and only at long times does the simulation trajectory match true analytical behaviour. This means it is crucial that all random numbers generated over the course of the simulation are independent and identically distribution. The first stage in the calculation of $\delta r_{i\alpha}^G$ involves generation of a random number in the range $[0, 1)$ using the L'Ecuyer method with Bays-Durham shuffle [33]. This is then transformed into random number sampled from the required Gaussian distribution by the Box-Muller method [33].

The Brownian dynamics simulations I present are of a 500 particle ensemble in a cubic box of fixed volume. The particles are initialized randomly in the box and periodic boundary conditions are implemented. The inter-particle interaction is the Morse potential with $\rho_0 = 34.38\sigma^{-1}$ and $r_e = \sigma$ which is truncated for $r > 1.5\sigma$ using the same method employed in the Lennard-Jones simulations (c.f. section 2.1). The time-step is $\delta t = 0.005$ and all runs last for $4 \cdot 10^7$ steps. This corresponds to about $11\frac{1}{2}mins$ real time, which compares well with the $\sim 15mins$ long experimental observations of gelation which I am simulating. All other parameters are as table 1.

A tangible measure of the rate of diffusion is the average time taken for a colloid to diffuse its own radius, also known as the Brownian time. This is given by

$$\tau_B = \frac{\left(\frac{\sigma}{2}\right)^2}{2D}. \quad (14)$$

In experiments the Brownian time is shown as $\tau_B = 9.342s$ or $\tau_B = 2683 \left(\frac{m\sigma^2}{k_B T}\right)^{0.5}$ in simulation time units.

2.5 Classification of State Points as Gels, Fluids and Cluster Fluids

To identify the region of the phase diagram in which a state point lies, I examine the nature of the potential energy during the simulation. Runs in the fluid region have potential energy which has no trend visible through the noise. In the coexistence region the potential energy falls away exponentially over course the run

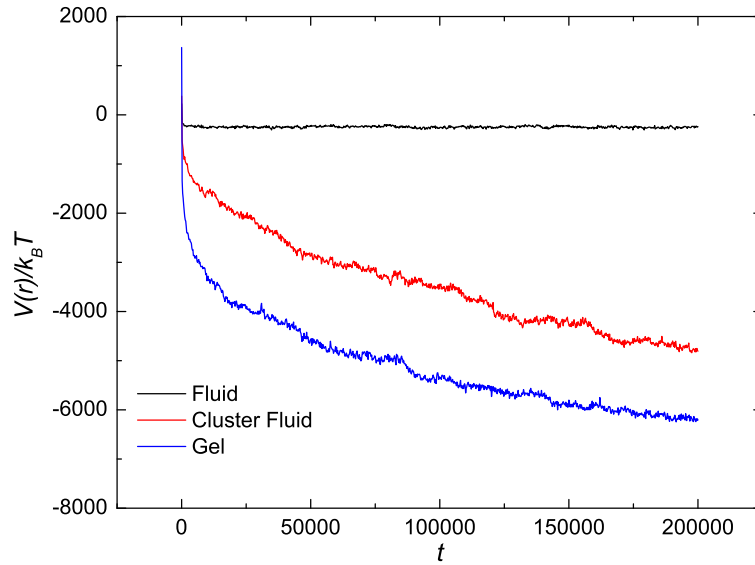


Fig. 7: **Classification of simulation into either fluid-crystal coexistence or fluid region of the phase diagram.** The potential energy of the simulated fluid (black line) is constant bar noise. Both coloured lines are simulations of non-ergodic states in the fluid-crystal coexistence region of the phase diagram. The exponential decay in potential energy is clear. The simulation state points which generated these potential curves were $\phi_c = 0.05$, $\epsilon = 2$ for the fluid (black line), $\phi_c = 0.05$, $\epsilon = 4$ for the cluster fluid (red line), and $\phi_c = 0.19$, $\epsilon = 4$ for the gel (blue line).

and corresponds to the cluster fluid and gel non-ergodic phases for our simulations. Both types of potential energy evolution are depicted in figure 7.

A method is devised to test whether a non-ergodic phase forms a structure which percolates through space, as seen in colloidal gels. A bond network is created by labeling atoms separated by a distance less than $r_B = 1.18$ as bonded. Initially I do not consider bonds with the periodic images of the simulation box. The value of r_B is chosen as the distance at which the Asakura-Oosawa potential decays to zero. The method works well with for the non-ergodic suspensions as these occur for bond strengths of multiple $k_B T$, meaning bonds lifetime is large. Towards the freezing line the binding energy of AO potential weakens ($\sim 2 - 3k_B T$) and thermal energy cause the particles to fluctuate between bonded and unbonded states. The boundary between what intuitively is a gel or a cluster fluid blurs. This is because the system transforms dynamically between the two states due to thermal fluctuations on simulation time scales.

Next the coordinates of the particles in the largest connect component of the bond network are extracted. This defines a new bond network for the largest cluster, to which periodic boundary conditions are applied. If one or members of the largest cluster is bonded through the walls of the simulation box to any members in the periodic images of the itself, the cluster is said to percolate. I only require percolation in one dimension to account for the finite size effect of the simulation.

In the coexistence region of the phase diagram, percolated clusters are identified as gels and those not are cluster fluids. The methods described are used to classify simulation state points as fluids, gels and cluster fluids.

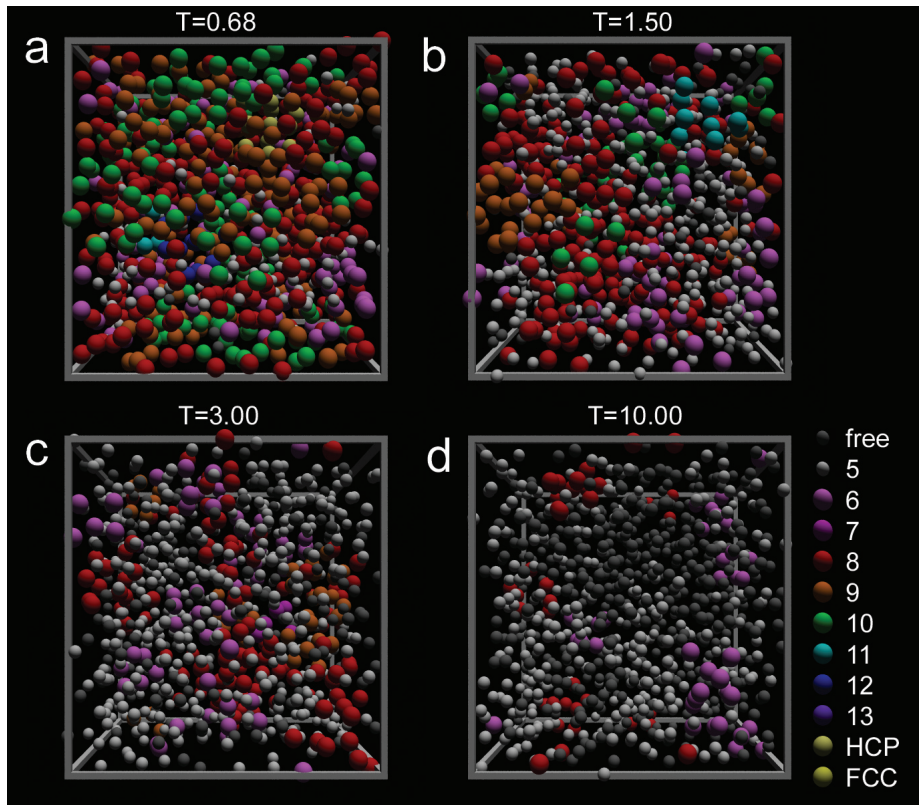


Fig. 8: **Simulation snapshots of Lennard-Jones fluid.** Particles which are identified as members of the Morse clusters are highlighted with colour, free particles are dark grey (c.f. key on figure). As the temperature drops it is evident that the fluids adopt local ordering. Images from simulation ensemble of 2048 particles, density $\rho = 0.850$ with temperature **a)** on triple point $T_F = 0.68$, **b)** $T_F = 1.50$, **c)** $T_F = 3.00$, **d)** as high temperature fluid, $T_F = 10.00$.

3 Results

3.1 Lennard-Jones Fluid Cluster Analysis

In total I simulate nine Lennard-Jones fluids, five of which are classified as liquids as their temperature falls below the critical value ($T_F < T_c \simeq 1.2$ [34]). All simulations are examined for local structure using the TCC algorithm as described in section 2.2. In figure 8 I highlight with colour particles identified as members of a Morse cluster, based on the size of the cluster and the type of 13 particle crystal fragment, in renderings of simulation ensembles. It is evident from the increasing colour of the renders that particles in low temperature fluids assemble into local structures.

To understand which clusters develop on cooling, I calculate average populations for the Morse and Lennard-Jones clusters. The measure used to this end is the ratio $\frac{N_{LFS}}{N}$ which is the number of particles N_{LFS} that are identified as members of a particular cluster type normalized by the number of particles considered $N = 2048 * 180$. It is best described as the relative frequencies of a given type of cluster accounted for by its number of constituents.

Figure 9a shows the evolution of local ordering. For a high temperature fluid, $T_F = 10.00$, around 20% of all particles are identified as members of a cluster (black diamonds and dotted black line). This increases to over 95% at the triple point $T_F = 0.68$. All the Morse clusters composed of 8 or more particles increase in popularity on cooling. It appears that this is at the expense of the smaller 5, 6 and 7 membered clusters which decrease in popularity between $T_F = 1.50$ and $T_F = 0.68$. The most popular cluster sizes at low temperatures

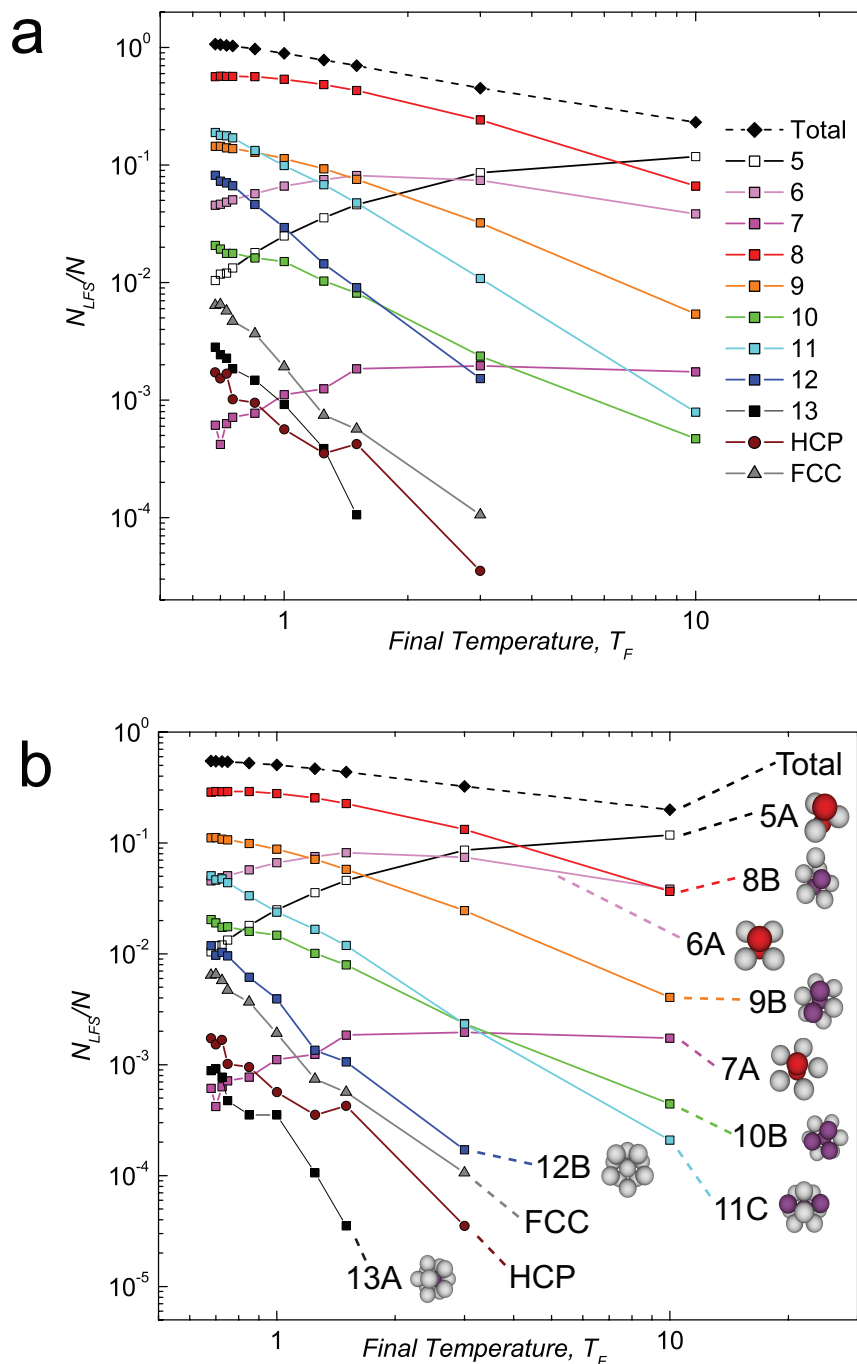


Fig. 9: **Proportion of particles identified in a particular class of cluster.** a) Particles identified in the Morse clusters of size 5 to 13 particles, and identified as the 13 particle FCC and HCP crystal fragments. b) Particles identified as Lennard-Jones global minimum LFS and the $m = 13$ crystal fragments. In b) the structures of the Lennard-Jones LFS are drawn next to the corresponding population lines.

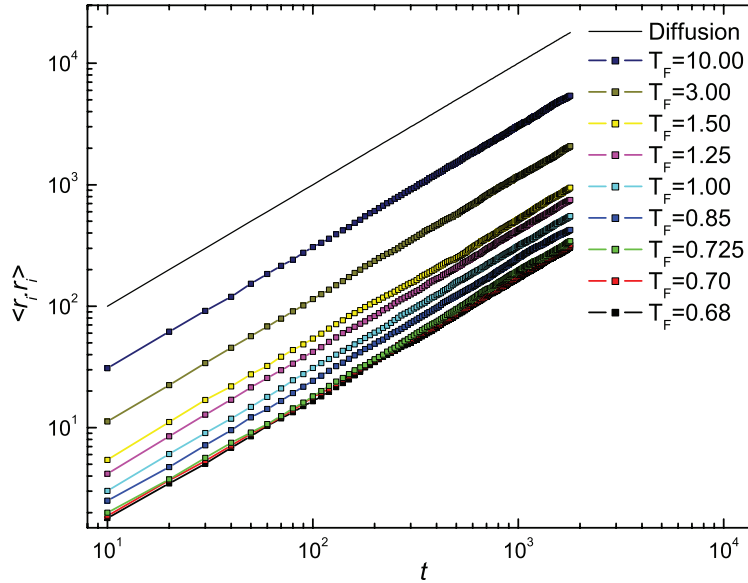


Fig. 10: **Mean squared displacement (MSD) of particles after equilibration.** The solid black line indicates a linear relationship between mean squared displacement and time. The ensemble mean squared displacements track this line confirming the fluids are diffusive. The diffusion constant D is calculated for each ensemble using eq 15.

consist of 6, 8, 9 and 11 particles.

The population graphs of Lennard-Jones clusters only are displayed in figure 9b. The graph is qualitatively similar to figure 9a, yet examination of the minutiae reveals some important results. I note for low temperatures, $T_F < 0.725$, that particles membered in Lennard-Jones clusters account for $\sim 54\%$ of all particles examined. This implies roughly 40% of particles are members of the non-Lennard-Jones Morse LFS for the same temperatures and justifies the detection of these clusters. This result arises from the fact that many Morse and Lennard-Jones LFS of the same size have quantitatively similar binding energies [28] so there is little thermodynamic impetus to rearrange as just Lennard-Jones LFS.

Perhaps the most important result derived from figure 9b relates to Frank's 1952 conjecture stated in section 1.2. The icosahedral LFS is observed to be less popular than either of the 13 particle crystal fragments. At most temperatures it is generally the case that icosahedra are the least common of all other Lennard-Jones clusters.

It is interesting to note the dependence of the popularity of the 6A crystal fragment on temperature. It increases in popularity in cooling from $T_F = 10.00$ and $T_F = 1.50$ but then decreases from its highest popularity at $T_F = 1.50$ on further cooling to $T_F = 0.68$. The other two smallest LFS, 5A and 7A, also decrease on cooling perhaps as a consequence of the increasing proportions of all clusters of 8 or more particles.

The three most popular Lennard-Jones LFS at the triple point are 8B, 9B and 10B, with their constituents comprising nearly 40% of all the particles detected in the Lennard-Jones clusters. The structures of the 8B, 9B and 10B clusters are based on the 7A pentagonal-bipyramids and possess symmetry which impedes crystal growth [11]. Although the 6A population decreases in the liquid regime, it is still a popular structure in absolute terms accounting for around 5% of the particles in Lennard-Jones clusters.

I next consider the lifetimes of the clusters by plotting the mean squared displacement (MSD) of the particles, figure 10. The logarithmic scale allows comparison of the ensemble mean squared displacements to a black reference line which indicates a linear proportionality between MSD and time. The simulation lines are all of the same gradient implying the fluids are diffusive. Application of Fick's second law of diffusion, like in section 2.4, gives the relationship $\langle \mathbf{r}_i, \mathbf{r}_i \rangle = 2Dt$. The diffusion constant D can be calculated from the gradient of the MSD by

$$D = \frac{1}{2} \frac{d}{dt} \langle \mathbf{r}_i, \mathbf{r}_i \rangle . \quad (15)$$

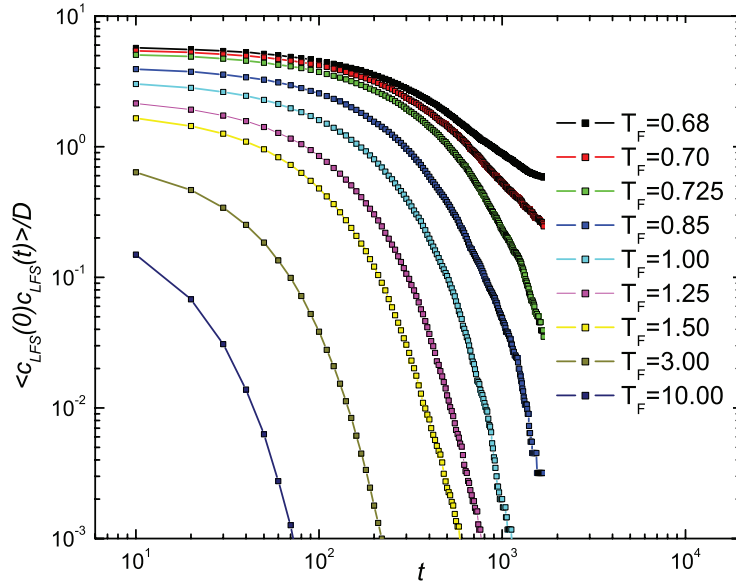


Fig. 11: **Morse cluster lifetime correlation function scaled by diffusion constant.** As the temperature increases the correlation functions fall away at shorter times, indicating that the Morse clusters must break up at some point of the simulation.

I find the diffusion constant D for each fluid simulation by calculating a linear regression line for the MSD state points and finding the gradient.

I measure the stability of the Morse clusters using the lifetime correlation function $\langle c_{LFS}(0)c_{LFS}(t) \rangle$ defined in [6]. This is based on the residency of individual particles in a Morse cluster; the correlation $c_{LFS}(t) = 1$ if a particle resident in a cluster at time 0 is still resident in a cluster at time t , otherwise $c_{LFS}(t) = 0$ ². I scale the correlation function by the diffusion constant to compensate for faster diffusion in high temperature ensembles causing the dynamics to evolve quicker than at low temperatures.

Figure 11 plots the lifetime correlation function. I note that as temperature increases, the correlation functions begin to fall away at shorter times. This indicates that the particles identified in Morse clusters at time 0 free from their groupings in a cluster during the simulation and consequently the those clusters must be break up during the simulation. However this does not mean that freed particles do not go on a become part of another cluster at a later stage. It just implies that cluster based structures in liquids are not static and change dynamically.

Solidification of clusters is indicated by a correlation function which remains constant for the entire duration of a simulation. The macroscopic form of this local solidification may be crystal or the non-ergodic phases of glasses, gels or cluster fluids. The type would depend on mainly on the simulation parameters, with some dependence on initial configuration as well.

² Here I consider $t = 0$ as the end of the equilibration phase of the simulations.

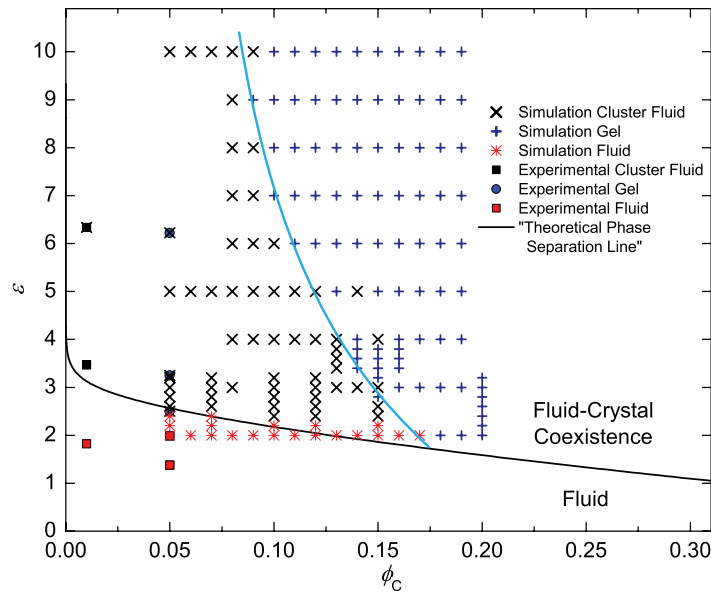


Fig. 12: **Phase space for the colloidal dispersion.** Experimental state points are shapes, simulation state points are crosses and phase separation is the black line. The light blue line indicates an empirical estimation of where the simulation percolation line falls. State points $(\phi_c = 0.05, \epsilon = 2.5)$, $(\phi_c = 0.05, \epsilon = 3.246)$ and $(\phi_c = 0.05, \epsilon = 6.226)$ are all experimental colloidal gels. They lie well inside the cluster fluid region of the simulations, and in fact simulations of identical state points form cluster fluids and not gels. The simulations appear to track the phase separation line predicted by free volume theory [25].

3.2 Brownian Dynamics Simulation of Gels

I simulate approximately 150 state points of the phase diagram in order to find the percolation line for the model dispersions. Figure 12 is a plot of the phase diagram where simulation state points are labeled with crosses. The three types of coloured cross represent the fluid, cluster fluid and gel phases discussed in section 1.3 and depicted in figure 3. Experimental data is also plotted as shapes, where the same colour scheme is also used to indicate phase. The black line is the phase separation line generated from free volume theory [25]. The underlying equilibrium state for the section of the graph above the phase separation line is fluid-crystal coexistence. The simulations undergo a liquid to non-ergodic (gel of cluster fluid) phase transition on crossing this line.

The three experimental gel state points, $(\phi_c = 0.05, \epsilon = 2.5)$, $(\phi_c = 0.05, \epsilon = 3.246)$ and $(\phi_c = 0.05, \epsilon = 6.226)$ are all simulated. The simulations do not form gels but cluster fluids and the discrepancy is evident on figure 12 due to a clash of colours at these state points. In fact it is evident from grid-wise sampling of state points that the percolation line falls at much higher colloid volume fraction ϕ_c for simulations than in the experiments. The experimental results indicate the gel percolation line approximately between the bounds of 1% and 5% volume fraction in the area of the phase diagram explained. Conversely the simulations never form gels for colloid volume fractions lower than 9% and empirically I see that the percolation line falls between 9% and 17% depending on epsilon ϵ . I have fitted an approximate simulation gel percolation line to the phase diagram with a light blue line.

Figure 13a depicts snapshots of the state point $(\phi_c = 0.05, \epsilon = 6.226)$ for the experimental gel. This compares with figure 13b, a render of the final coordinate set for a simulation of the same state point. The simulation forms a cluster fluid which does not percolate as a gel would.

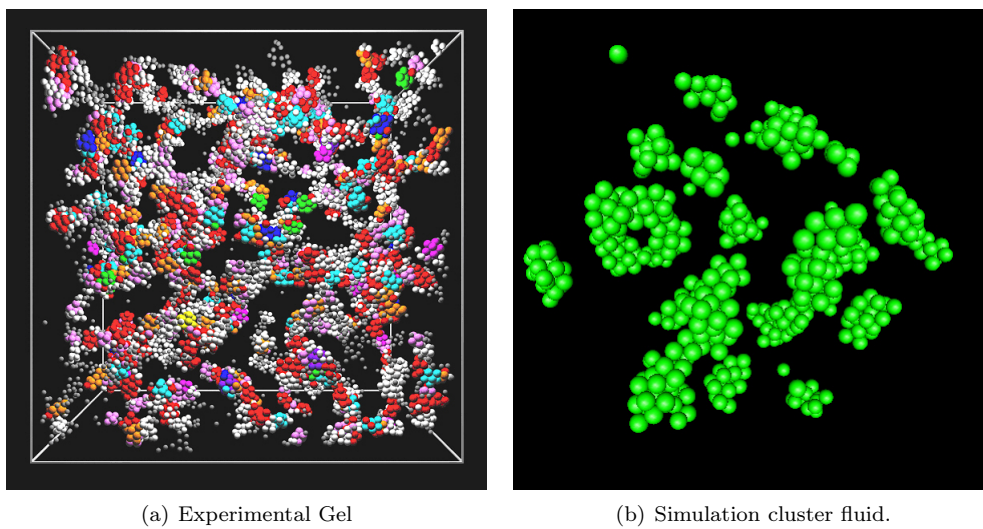


Fig. 13: **Comparison of experimental state point which gels yet simulation does not.** Both pictures of the same state point, ($\phi_c = 0.05, \epsilon = 6.226$). **a)** is an experimental gel of 5098 particles. The individual particle coordinates are interpolated from confocal microscope images of the experiment (like figure 2) and rendered with the Morse clusters highlighted with colour [6]. **b)** is the Brownian dynamics simulation of the same state point. This is a cluster fluid which, for the duration of the simulation, does not form percolating arms of colloids between clusters needed to make a gel.

4 Conclusions and Future Research Directions

The application of the topological cluster classification algorithm to the trajectories of Lennard-Jones systems have shown that locally favoured structures are ubiquitous in the liquid phase. Almost all particles in the liquid phase are identified as members of one of the $m = 5$ to $m = 13$ Morse clusters. Just over half of these particles are actually members of the Lennard-Jones global minimum locally favoured structures, whilst the others are either non-Lennard-Jones Morse locally favoured structures or thirteen particle crystal fragments. This shows that the Lennard-Jones LFS are not automatically preferred and fluid particles explore other thermodynamically favourable structures. I note for liquids that the most prevalent clusters contain 8 particles, with 6, 9 and 11 particle clusters also frequently seen. Clusters of 7 and 13 particles are rare in comparison, meaning there is something unfavourable about the process in which they self-assemble.

It appears Frank was incorrect on two counts with his 1952 conjecture. I do identify the presence icosahedral clusters in the liquids, however they are extremely rare and less popular than the two other distinct arrangements of twelve particles around a central particle (FCC and HCP crystal fragments). However the populations of icosahedra may become more significant on cooling below the freezing. The pentagonal-bipyramid based structures, $8B$, $9B$ and $10B$, possess five-fold symmetry and may prove more prohibitive to crystal growth in liquids than icosahedra by virtue of their sheer numbers. By virtue of their popularity, it is natural to extend this analysis to determine the relative proportions of each of the non-Lennard-Jones Morse LFS and see whether they are mainly crystalline or five-fold symmetric in structure. To improve the accuracy of the results for the relative proportions of each cluster type, ensemble computation of multiple liquid simulations with different initial conditions could generate statistics on the populations.

The bond orientational order parameter W_6 [11] can be used to estimate the extent to which cluster structure is incompatible with bulk crystal formation. This idea could be combined with the relative populations of cluster type to predict the ensembles which crystallize and those which undergo vitrification. The scope of this idea could be broadened to include simulations of other potentials which are known to be better glass formers than Lennard-Jones. Examples of these include the Morse potential and the Johnson potential [14].

An interesting extension to this work would involve bringing the simulation temperature down through the freezing line to see how local structure in liquids reorders as the system begins to phase separate. This would determine if the W_6 -based inferences on crystallization and vitrification actually manifest in the dynamics.

The flow of particles in liquids slow upon cooling and one could examine the cluster lifetime correction function to investigate the effect cooling liquids below freezing has on reordering of clusters. Viewing sequential renderings of simulation snapshots, with individual clusters highlighted with colour, could reveal how the dynamics of clusters affect the formation of metastable solid states.

The main result noted from the Brownian dynamics simulation of gelation is that the location of the percolation line on the phase diagram, as identified by the simulation state points, is markedly different to the experimental percolation line. I try identify possible origins for this discrepancy, the first of which could be a simple finite size effect. The simulations only model 500 colloids compared to the thousands observed in the experiments through the confocal microscope. The volume of the simulation ensembles means that the cluster fluids witnessed at the experimental gelation state points may fit within one of the voids contained inside the percolated network of colloids forming the experimental gels. These voids often contain unbounded clumps of clusters due to the underlying ground state of fluid-crystal phase separation.

It could be the case that the Brownian dynamics runs happen to only simulate the voids. Statistically it seems improbable that none of the ~ 50 simulated state points of the experimental gel region of the phase diagram would only simulate voids and not fractions of the gel network by chance alone. This is especially unlikely for the higher volume fractions where the size of the voids shrink as more space becomes occupied with colloids. As the execution time of my simulation code scales linearly with simulation size it would be easy to increase the size of the Brownian dynamics simulations towards 5000 particles to confirm this intuition³.

I believe it is more likely that the model for the colloidal dispersion is itself inaccurate. I note four possible sources of error:

1. Simulation of monodisperse particles when the colloids actually have a 4% polydispersity.
2. No inclusion of electrostatic charge effects between colloids.

³ The 500 particle simulation size was originally chosen for quick sampling of phase space.

3. In mapping the Morse potential onto the Asakura-Oosawa potential I qualitatively change the dynamics of the system.
4. The hydrodynamic interactions between the colloids and the solvent are highly non-linear and do not simplify to just Brownian motion of the colloids on long time-scales.

The first two factors listed are simple perturbations to the system which could be incorporated in the simulation easily. In fact the experimental dispersions are designed in a manner to control these two factors as well as practically possible, so it seems unlikely that they would be crucial to gelation.

The third point belies the main motivations for using the Morse potential in the simulations. It is almost trivial to design a steeper potential with a faster change in gradient at $r = \sigma$ as a better match for Asakura-Oosawa interaction. This could also rid us of the approximation incorporated in having a fixed range parameter ρ_0 for all reservoir packing fractions η_p^r . However ensuring numerical stability of the simulations becomes more difficult. A small value of δt is needed to ensure that particles do not overlap to the extent that the forces grow larger than what is practically computable. In other words the simulations are liable to blow up at large δt . The issue is discussed in more detail in [4, 9], but to use a small value for δt means that simulation of experimental length timescales quickly becomes unfeasible even with a modern supercomputer.

The fourth point poses the question how best to account for the colloid-solvent interactions. The affect of one molecule on another due to the flow of solvent particles around them is complex in itself. A large ensemble of colloids interacting with spies of similar size, such as a two clumps of clusters flowing past each other is extremely non-linear [35]. Ermak and McCammon introduced a method to incorporate hydrodynamic effects into Brownian dynamics simulations by utilizing the Oseen tensor to model pairwise interactions between colloids mediated by solvent flow [24]. An implementation of this in a Brownian dynamics simulation of a colloidal gel would be of great interest.

It may be necessary to explore the effect of all these factors, both individually and in combination, before the origin of the percolation line discrepancy is resolved.

5 Acknowledgments

Foremost, I would like to thank Paddy Royall for the amount time he has invested in the supervision this project, and for his seemingly inexhaustible patience to re-explain concepts and ideas to me. Secondly thanks to Jens Eggers, for the logical manner in which he has considered my research and for the clarity of his suggestions. Without the topological cluster classification much of this work would not have been possible, for which I am indebted to Stephen Williams. In addition I am very grateful to Hajime Tanaka, of the Soft Matter Tanaka Laboratory, Institute of Industrial Science, University of Tokyo for hosting me in his laboratory during a very productive month long research placement in Japan. The funding which realized this trip was awarded to me by John Hogan in his capacity as director of the Bristol Centre for Complexity Sciences, whom I am also thankful. More thanks to Rob Jack and Takeshi Kawasaki for enlightening discussions during the course of this research.

References

- [1] Hansen, J.-P. & Macdonald, I. *Theory of Simple Liquids* (London: Academic press, 1976).
- [2] Frank, F. C. Supercooling of liquids. *Proc. R. Soc. Lond. A.* **215**, 43–46 (1952).
- [3] Lennard-Jones, J. E. Cohesion. *Proceedings of the Physical Society* **43**, 461–482 (1931). URL <http://stacks.iop.org/0959-5309/43/461>.
- [4] Frenkel, D. & Smit, B. *Understanding Molecular Simulation: from Algorithms to Applications* (New York: Academic, 2001).
- [5] Williams, S. R. Topological classification of clusters in condensed phases. *to be published* (2007).
- [6] Patrick Royall, C., Williams, S. R., Ohtsuka, T. & Tanaka, H. Direct observation of a local structural mechanism for dynamic arrest. *Nat Mater* **7**, 556–561 (2008). URL <http://dx.doi.org/10.1038/nmat2219>.
- [7] Asakura, S. & Oosawa, F. On interaction between two bodies immersed in a solution of macromolecules. *J. of Chem. Phys.* **22**, 1255–1256 (1955).
- [8] Poon, W. C. K. The physics of a model colloid-polymer mixture. *J. Phys. Cond. Mat.* **14**, R859–R880 (2002).
- [9] Allen, M. P. & Tildesley, D. J. *Computer Simulation of Liquids* (Oxford University Press, 1989).
- [10] Hansen, J.-P. & Verlet, L. Phase transitions of the lennard-jones system. *Phys. Rev.* **184**, 151–161 (1969).
- [11] Steinhardt, P. J., Nelson, D. R. & Ronchetti, M. Bond-orientational order in liquids and gases. *Phys. Rev. B* **28**, 784–805 (1983).
- [12] Honeycutt, J. D. & C., A. H. Molecular dynamics study of melting and freezing of small lennard-jones clusters. *J. Phys. Chem.* **91**, 4950–4963 (1987).
- [13] LaViolette, R. A. & Stump, D. M. Local structural motifs in a quenched model monatomic liquid. *Phys. Rev. B* **50**, 5988–5998 (1994).
- [14] Tomida, T. & Egami, T. Molecular-dynamics study of orientational order in liquids and glasses and its relation to the glass-transition. *Phys. Rev. B* **52**, 3290–3308 (1995).
- [15] Reichert, H. *et al.* Observation of five-fold local symmetry in liquid lead. *Nature* **408**, 839–841 (2000).
- [16] Di Cicco, A., Trapananti, A., Faggioni, S. & Filipponi, A. Is there icosahedral ordering in liquid and undercooled metals? *Phys. Rev. Lett.* **91**, 135505 (2003).
- [17] Wales, D. J. *Energy Landscapes: Applications to Clusters, Biomolecules and Glasses* (Cambridge University Press, Cambridge, 2004).
- [18] Doye, J. P. K., Wales, D. J. & Berry, R. S. The effect of the range of the potential on the structures of clusters. *J. Chem. Phys.* **103**, 4234–4249 (1995).
- [19] Mezzenga, R., Schurtenberger, P., Burbidge, A. & Michel, M. Understanding foods as soft materials. *Nat Mater* **4**, 729–740 (2005). URL <http://dx.doi.org/10.1038/nmat1496>.
- [20] Hunter, R. J. *Foundations of Colloid Science* (Oxford University Press, 2001).
- [21] van Blaaderen, A. & Wilzius, P. Real-space structure of colloidal hard-sphere glasses. *Science* **270**, 1177 (1995).
- [22] Zaccarelli, E. Colloidal gels: equilibrium and non-equilibrium routes. *Journal of Physics: Condensed Matter* **19**, 323101 (50pp) (2007). URL <http://stacks.iop.org/0953-8984/19/323101>.

-
- [23] Lu, P. J. *et al.* Gelation of particles with short-range attraction. *Nature* **453**, 499–503 (2008). URL <http://dx.doi.org/10.1038/nature06931>.
- [24] Ermak, D. L. & McCammon, J. A. Brownian dynamics with hydrodynamic interactions. *The Journal of Chemical Physics* **69**, 1352–1360 (1978). URL <http://link.aip.org/link/?JCP/69/1352/1>.
- [25] Lekkerkerker, H. N. W., Poon, W. C. K., Pusey, P. N., Stroobants, A. & Warren, P. B. Phase-behavior of colloid plus polymer mixtures. *Europhys. Lett.* **20**, 559–564 (1992).
- [26] Hoover, W. G. Canonical dynamics: Equilibrium phase-space distributions. *Phys. Rev. A* **31**, 1695–1697 (1985).
- [27] Morse, P. M. Diatomic molecules according to the wave mechanics ii: vibrational levels. *Phys. Rev.* **34**, 57–64 (1929).
- [28] Doye, J. *et al.* Controlling crystallization and its absence: Proteins, colloids and patchy models. *Phys. Chem. Chem. Phys.*, DOI: **10.1039**, b614955c (2007).
- [29] Bernal, J. D. & Finney, J. L. Random close-packed hard-sphere model. ii. geometry of random packing of hard spheres. *Discussions of the Faraday Society* **43**, 62–69 (1967).
- [30] Franzblau, D. S. Computation of ring statistics for network models of solids. *Phys. Rev. B* **44**, 4925–4930 (1991).
- [31] Dijkstra, M., Brader, J. M. & Evans, R. Phase behaviour and structure of model colloid-polymer mixtures. *Journal of Physics Condensed Matter* **11**, 10079–10106 (1999).
- [32] Noro, M. G. & Frenkel, D. Extended corresponding-states behavior for particles with variable range attractions. *The Journal of Chemical Physics* **113**, 2941–2944 (2000). URL <http://link.aip.org/link/?JCP/113/2941/1>.
- [33] Press, W. H., Flannery, B. P., Teukolsky, S. A. & Vetterling, W. T. *Numerical Recipes in C, Second Edition* (Cambridge Univ. Press, Cambridge, 1992).
- [34] Wilding, N. Critical-point and coexistence-curve properties of the lennard-jones fluid: A finite-size scaling study. *Phys. Rev. E.* **52**, 602–611 (1995).
- [35] Batchelor, G. K. & Green, J. T. The determination of the bulk stress in a suspension of spherical particles to order c_2 . *Journal of Fluid Mechanics* **56**, 401–427 (1972).